RESEARCH ARTICLE

Coordination Polymer Electrocatalysts Enable Efficient CO-to-Acetate Conversion

Mingchuan Luo, Adnan Ozden, Ziyun Wang, Fengwang Li, Jianan Erick Huang, Sung-Fu Hung, Yuhang Wang, Jun Li, Dae-Hyun Nam, Yuguang C. Li, Yi Xu, Ruihu Lu, Shuzhen Zhang, Yanwei Lum, Yang Ren, Longlong Fan, Fei Wang, Hui-hui Li, Dominique Appadoo, Cao-Thang Dinh, Yuan Liu, Bin Chen, Joshua Wicks, Haijie Chen, David Sinton, and Edward H. Sargent*

Upgrading carbon dioxide/monoxide to multi-carbon C_{2+} products using renewable electricity offers one route to more sustainable fuel and chemical production. One of the most appealing products is acetate, the profitable electrosynthesis of which demands a catalyst with higher efficiency. Here, a coordination polymer (CP) catalyst is reported that consists of Cu(I) and benzimidazole units linked via Cu(I)-imidazole coordination bonds, which enables selective reduction of CO to acetate with a 61% Faradaic efficiency at −0.59 volts versus the reversible hydrogen electrode at a current density of 400 mA cm^{-2} in flow cells. The catalyst is integrated in a cation exchange membrane-based membrane electrode assembly that enables stable acetate electrosynthesis for 190 h, while achieving direct collection of concentrated acetate (3.3 molar) from the cathodic liquid stream, an average single-pass utilization of 50% toward CO-to-acetate conversion, and an average acetate full-cell energy efficiency of 15% at a current density of 250 mA cm^{-2}.

1. Introduction

The electrocatalytic production of valuable multi-carbon (C_{2+}) fuels and chemicals from CO_2/CO has the potential to enable the chemical industry to utilize intermittent renewable electricity to power the progressive replacement of fossil sources of chemicals with renewable/low-carbon ones.[1–4] Catalysts steer these processes toward desired products, desirably with high selectivity and energy efficiency.[5–7] Cu-based materials upgrade CO_2/CO feedstocks to C_{2+} products,[8–11] among which acetate is an important industrial product with an annual production volume of ≈7 million tonnes and a forecast global market of 22 billion USD by 2027.[12–14] A

M. Luo, Z. Wang, F. Li, J. Erick Huang, S.-F. Hung, Y. Wang, J. Li, D.-H. Nam, Y. C. Li, Y. Lum, C.-T. Dinh, Y. Liu, B. Chen, J. Wicks, H. Chen, E. H. Sargent
Department of Electrical and Computer Engineering
University of Toronto
35 St, George Street, Toronto, Ontario M5S 1A4, Canada
E-mail: ted.sargent@utoronto.ca
A. Ozden, J. Li, Y. Xu, D. Sinton
Department of Mechanical and Industrial Engineering
University of Toronto
5 King's, College Road, Toronto, Ontario M5S 3G8, Canada
Z. Wang, R. Lu
School of Chemical Sciences
The University of Auckland
Auckland 1010, New Zealand
F. Li, S. Zhang
School of Chemical and Biomolecular Engineering and The University of Sydney Nano Institute
The University of Sydney
Sydney, NSW 2006, Australia

S.-F. Hung
Department of Applied Chemistry
National Yang Ming Chiao Tung University
Hsinchu 300, Taiwan
Y. Lum
Institute of Materials Research and Engineering
Agency for Science
Technology and Research (A*STAR)
2 Fusionopolis Way, Innovis, Singapore 138634, Singapore
Y. Ren, L. Fan
X-ray Science Division
Argonne National Laboratory
Lemont, Illinois 60439, USA
F. Wang
State Key Laboratory of Coal Conversion, Institute of Coal Chemistry
Chinese Academy of Sciences
Taiyuan 030001, P. R. China
H.-h. Li
Key Laboratory for Ultrafine Materials of Ministry of Education
School of Chemical Engineering
East China University of Science and Technology
Shanghai 200237, China
D. Appadoo
Australian Synchrotron-ANSTO
Clayton, VIC 3168, Australia

**ADVANCED
SCIENCE NEWS**

www.advancedsciencenews.com

**ADVANCED
MATERIALS**

www.advmat.de

recent techno-economic analysis suggests that the electrosynthesis of acetate from CO_2-derived CO could become economical once sufficient selectivity, reaction rate, and stability are realized.[15]

In order to advance the electroproduction of acetate in the direction of practical application, electrocatalysts must facilitate C–C coupling in a manner that favors acetate by suppressing other C_{2+} products, such as ethylene, ethanol, and propanol.[16–20] We report herein a coordination polymer (CP) strategy that leads to efficient CO-to-acetate conversion. The inspiration for this approach came from the corrosion field, in which Cu-based CPs have been found to enable anti-corrosion properties in dynamic chemical/electrochemical environments.[21] The specific choice of 1D Cu(I)-benzimidazole CP was motivated by previous finding that only this structure can be found on CP-modified Cu electrodes after CO_2 electrolysis in an H-type cell.[22] Electrochemical and in situ spectroscopic analyses were applied to characterize the chemical and structural stability of the CP catalyst during the CO reduction reaction (CORR). Density functional theory (DFT) calculations provide evidence for the thermodynamic stability of the CP catalyst, a factor that prevents decomposition of ligand-Cu(I) units to form metallic clusters. Performance, tested in a gas diffusion electrode-based flow cell system, shows that CP catalysts provide a Faradaic efficiency (FE) of 61% for CO-to-acetate conversion at a current density of 400 mA cm^{-2} and at a potential of −0.59 V versus the reversible hydrogen electrode (RHE).

We screened the energetics of adsorption configurations of possible intermediates on CP with DFT and explored options for catalytic sites that have the potential to facilitate C–C coupling and favor acetate generation. In a membrane electrode assembly (MEA) using a cation exchange membrane (CEM),[23] we achieve stable acetate electrolysis for 190 h at a partial current density of 128 mA cm^{-2} and the direct collection of concentrated acetate (3.3 molar) from the cathodic liquid stream. This system maintains an average single-pass CO-to-acetate conversion of 50% and an average acetate full-cell energy efficiency of 15% throughout the 190 h initial reliability study.

2. Results and Discussion

2.1. Synthesis and Characterization

The CP catalyst – consisting of Cu(I) and benzimidazole units linked via Cu-imidazole coordination bonds – was synthesized using a wet-chemical approach. A mixture of commercial 25-nm Cu nanoparticles (NPs), benzimidazole (BIM-H) and ethanol was heated at 60 °C for 12 h (**Figure 1**a, details in Supporting Information). The formation of the CP involves the initial oxidation of metallic Cu to Cu(I), the subsequent coordination with both nitrogen atoms in the imidazole ring, and a final polymerization step.[21,22] Electron microscopy images show that the product is dominated by 1D nanowires (NWs). (Figure 1b; Figure S1a, Supporting Information). Scanning transmission electron microscopy (STEM) elemental mapping shows a homogeneous distribution of Cu and N throughout the NWs (Figure 1c). The Cu-to-N ratio was determined using inductively coupled plasma atomic emission spectroscopy

(ICP-AES, 1-to-2.07) and X-ray photoelectron spectroscopy (XPS, 1-to-2.22), and the measured ratio agrees well with the theoretically-predicted value 1:2 (Figure S1b, Supporting Information). Synchrotron X-ray diffraction (XRD) studies of the samples show the emergence of a crystalline phase distinct from Cu, Cu_2O and CuO (Figure S1c, Supporting Information), consistent with substantially complete conversion of the Cu NP precursor, also supported by TEM and Raman studies (Figure S1d,e, Supporting Information). Initial scale-up studies show that the synthesis method allows for gram-level production of CP NWs (Figure S2, Supporting Information).

We examined the electronic and chemical structure of as-synthesized CP samples. Figure 1d shows the X-ray absorption near-edge spectrum (XANES) at the Cu K-edge. Compared to standard copper materials, CP shows a similar absorption onset and white line energy to Cu_2O. The rising-edge shift (8981.7 eV) at the Cu K-edge suggests the +1 oxidation state of Cu in the CP. This agrees well with Cu $2p$ XPS and Cu LMM Auger spectra (Figure S1f,g, Supporting Information).[24] Extended X-ray absorption fine structure (EXAFS) fitting using a model structure of CP (Figure S3 and Table S1, Supporting Information) also supports two-coordination copper with a linear arrangement.[25,26] EXAFS further reveals the Cu−N coordination in the first shell path and the Cu-C in the second shell path (Figure 1e). Fourier-transform infrared spectroscopy (FTIR) and Raman studies indicate the preservation of imidazole and benzene rings of BIM, the deprotonation of -NH in imidazole, and the formation of a Cu−N bond in the as-synthesized CP sample (see Figures S4 and S5, Supporting Information for detailed peak assignment and analysis).[27,28] XPS N $1s$ spectrum of BIM-H shows two peaks located at 399.1 eV and 400.5 eV, respectively, which we associate with the different bonding environments of the two nitrogen atoms in BIM-H (Figure 1f and Figure 1h).[29] The close integral areas of these two peaks are consistent with the chemical structure of BIM-H.[30] The single peak at 398.8 eV for the CP suggests that the two nitrogen atoms are indistinguishable and are coordinated with Cu(I). Solid-state nuclear magnetic resonance (NMR) of the CP displays a downfield shift for the imidazole carbon 4 nucleus (as indicated in Figure 1g and Figure 1h) compared to the imidazole monomer spectrum (Figure 1i). This we assign to the addition of a positively charged nucleus in close proximity to the carbon 4 nucleus, as apparent in the chemical structure (Figure 1g). The broadening of the carbon 4 chemical shift of the imidazole is also indicative of the binding of nearby quadrupolar nuclei, such as ^{63}Cu or ^{65}Cu, which causes faster transverse relaxation of the carbon nucleus, leading to a shorter T2 and a broader signal. The characterization agrees with the picture that the building units of the CP samples are Cu(I) and benzimidazole linked via Cu-imidazole coordination bonds.

2.2. Investigation of Catalyst Stability

Next we examined, using electrochemical and in situ spectroscopy, the chemical and structural stability of CP catalyst under reducing potentials. We began by investigating its electrochemical properties in acetonitrile using 0.1 M tetrabutylammonium hexafluorophosphate as the supporting electrolyte. The use of
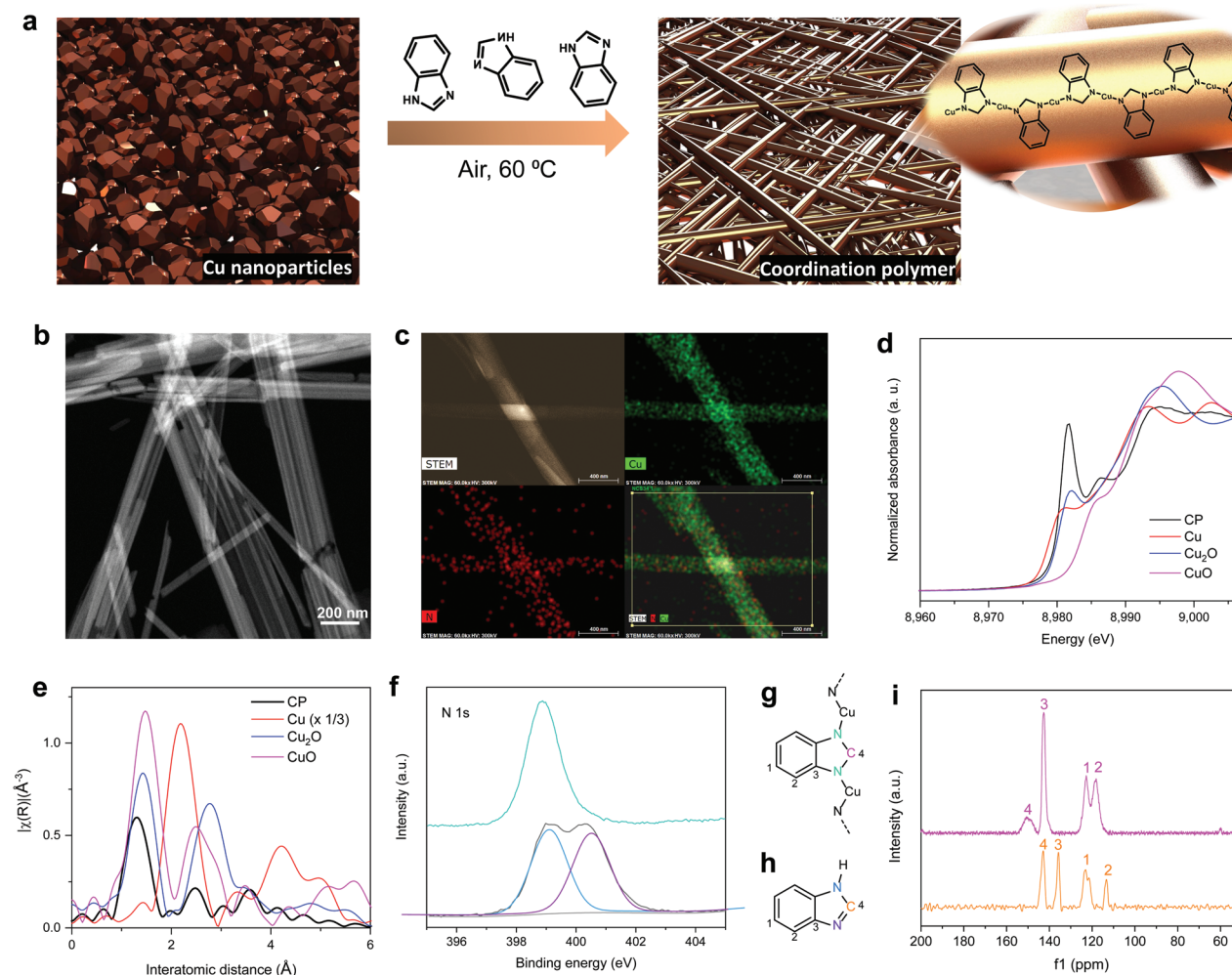
Figure 1. Synthesis and structural characterization of coordination polymer (CP) catalyst. a) Schematic of the synthesis process for CP. b) High-angle annular dark-field scanning transmission electron microscopy (HAADF-STEM) image and c) corresponding elemental mapping of CP nanowires. d) Cu K-edge X-ray absorption spectroscopy and e) Fourier transform of the experimental EXAFS spectra of CP catalyst, Cu, Cu_2O, and CuO. f) N 1s XPS spectra and i) Solid-state ^{13}C NMR spectra of CP and benzimidazole (BIM-H). g) Chemical structure of CP and h) BIM-H.

a non-aqueous electrolyte avoids interference arising due to water reduction with the study of redox properties. We found that the CP catalyst was not reduced until the applied potential was more negative than −1.35 V versus the normal hydrogen electrode (NHE) (**Figure 2**a). In comparison, the reduction of electrochemically-oxidized Cu NPs occurs from −0.17 V versus NHE (Figure S6a, Supporting Information). Similarly, in aqueous 1 M KOH electrolyte, no reduction peak was observed at the potential window associated with the reduction of copper oxides (Figure S6b, Supporting Information). These observations suggest higher stability of the CP catalyst against electrochemical reduction compared to electrochemically oxidized Cu NPs.

We monitored, using in situ Raman spectroscopy in a custom flow cell (Figure S7, Supporting Information),[31] the structure of the CP catalyst at a constant potential of −2 V versus Ag/AgCl with 1 M KOH. We found that the Raman spectrum characteristics, taken at different locations on the electrode, persisted in the case of the CP catalyst for over 15 h (Figure 2b; Figure S8a, Supporting Information). Minor changes between

1000 and 1300 cm^{-1} originate from interference of $KHCO_3$, generated from the side reaction between KOH and CO_2, over the course of extended operation (Figure S8b, Supporting Information). We also found that the Raman shift of the -NH in-plane bending (1138 cm^{-1}) did not appear in alkaline or neutral electrolyte (Figure S8c, Supporting Information), indicating that CP catalyst was stable and did not decompose into metallic Cu and BIM-H. We further conducted in situ X-ray absorption spectroscopy (XAS) on CP catalyst supported on a gas diffusion electrode in a flow cell in the presence of CO at a constant current density of 200 mA cm^{-2}. No obvious change in the oscillatory behavior was observed in in situ XANES (Figure 2c). Based on the energy derived from the zero-point value in the second-derivative spectra of in situ XANES (Figure S9a,b, Supporting Information), we found that the oxidation state of Cu in the CP catalyst remained near +1, further suggesting the chemical state stability of the CP catalyst under CORR. In contrast, Cu_2O catalysts were completely reduced to metallic Cu within 40 sec at a current density of −100 mA cm^{-2} under similar test conditions (Figure S9c–e, Supporting Information). We further
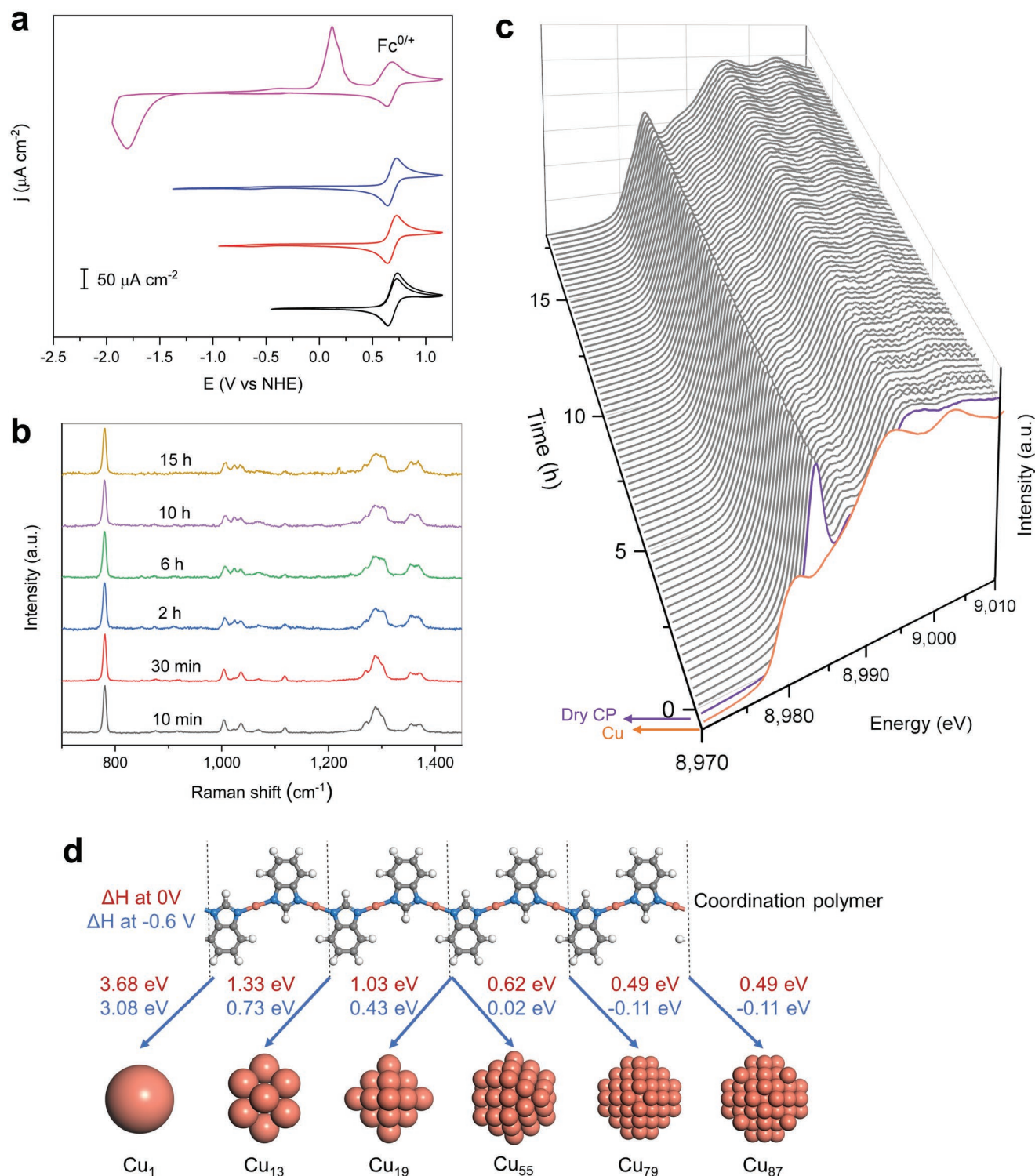
Figure 2. Structural stability of CP catalyst in CORR conditions. a) Cyclic voltammetry curves for CP catalyst in non-aqueous electrolyte. The redox of Fc/Fc+ occurring at 0.69 V versus NHE in acetonitrile was used as the internal standard. b) In situ Raman spectra of CP catalyst operating at −2 V versus Ag/AgCl in a flow cell. c) In situ Cu K-edge X-ray absorption spectroscopy of CP catalyst operating at −200 mA cm^{-2} under CORR conditions for over 18 h. d) Geometries of CP catalyst and copper nanoclusters within 100 atoms. The enthalpy changes of benzimidazole-Cu(I) reduction to each copper nanocluster per copper atom at 0 V (red) and −0.6 V (blue) versus RHE are listed.

acquired X-ray absorption near edge structure (XANES) of Cu L-edge and N K-edge of the CP catalyst under total electron yield (TEY) mode. This mode enables a surface resolution of ≈2 nm of the catalyst (Figure S9f,g, Supporting Information).

**ADVANCED
SCIENCE NEWS**

www.advancedsciencenews.com

**ADVANCED
MATERIALS**

www.advmat.de

We found no apparent change in XANES of both Cu L-edge and N K-edge of CP catalyst following reaction. By comparing the spectrum of the CP catalyst to the spectra of control samples, we checked for, and saw no presence of, evidence of metallic Cu, Cu_2O, and CuO species in the near-surface region of CP catalyst. We also collected surface-sensitive synchrotron THz far-infrared (THz/far-IR) absorption spectra to characterize the lattice dynamics of macromolecular structure and metal–ligand interactions of CP structure. From this we conclude that the macrostructure and the Cu-N coordination of the CP catalyst remain substantially unaltered following after CORR (Figure S10, Supporting Information).

We carried out DFT calculations to study the apparent stability of the materials. Typically, under the highly reducing conditions of CORR, Cu (I) tends to be reduced to Cu^0, which then forms clusters and further grows into large Cu nanocrystals.[18,32] We calculated the enthalpy changes of agglomeration for different Cu cluster sizes (< 100 atoms) using the Wulff construction (Figure 2d; Table S2, Supporting Information). We found that, at 0 V versus RHE, CP catalyst is thermodynamically more stable compared to Cu clusters with positive enthalpy changes. At the experimentally optimum potential of −0.6 V versus RHE, the conversion of CP to metallic Cu clusters smaller than 79 atoms is unfavorable; while a slightly negative enthalpy change of −0.11 eV was found for CP reduction to Cu_{79} and Cu_{87}. The formation of a 0.83-nm Cu_{79} cluster requires the agglomeration of all copper atoms in the CP over a 45-nm length. Without stable intermediates of smaller clusters as seeds, the lengthwise agglomeration of Cu atoms is kinetically difficult, explaining the experimentally observed stability of the CP catalyst.

2.3. CORR Performance

We first assessed the CO electroreduction performance of CP catalyst using a three-compartment flow cell and included controls involving commercial 25-nm Cu NPs and Cu_2O NWs (Figure S11, Supporting Information). The working gas diffusion electrode (GDE) was prepared by spray-depositing a homogeneous solution of CP catalyst and Nafion ionomer onto a hydrophobic gas diffusion layer (GDL) (see Supporting Information for details). **Figure 3**a shows the product distribution and current densities as a function of applied potentials on CP catalyst in 3 M KOH. Across a wide range of applied potentials, we detected the full range of products typical of Cu catalysts, with the exception of propanol.[33–35] This suggests the C_3 pathway of CORR is militated against on the CP catalyst. Across the potential region investigated, acetate formation dominates and reaches a maximum FE of 61 ± 4% at −0.59 V versus RHE. A lower optimum overpotential for C_2H_4 than that for acetate indicates their different reactive pathways after C–C coupling, consistent with the findings of Jiao and co-workers.[16] We achieved a half-cell energy efficiency (EE) of 26 ± 2% for the electrosynthesis of acetate from CO (Table S2, Supporting Information). At potentials more negative than −0.59 V, acetate was the only liquid product detected in the catholyte: more negative potentials resulted in a decrease in the FE of C_2 products, along with an increase in the FE toward methane and hydrogen.

We examined the influence of alkalinity on acetate production for CP catalyst by testing in a series of KOH concentrations from 1 to 5 M (Figure 3b). We found that high alkalinity favors CO-to-acetate conversion – evidence of the positive shift in onset potential with increasing electrolyte pH (Figure S12, Supporting Information). This agrees with previous mechanistic studies that the formation of acetate proceeds through OH^- attack of an adsorbed ketene intermediate.[17,36] In 3 M KOH, we achieved a peak acetate partial current density of 243 mA cm^{-2} at −0.59 V. Engineering the electrode structure and operating conditions enabled further improvements in acetate productivity (see Supporting Information for details), achieving a partial current density of 470 mA cm^{-2} at −0.65 V versus RHE (Tables S3 and S4, Supporting Information). We used commercial Cu NPs and as-synthesized Cu_2O NWs (to exclude the effect of 1D morphology) as control catalysts, and obtained a lower selectivity toward acetate (< 25%) with notable amount of propanol formation for both catalysts. Compared to CP catalyst, Cu NPs and Cu_2O NWs showed a greater diversity in product distribution with a shift to ethylene and alcohols, respectively, under similar reaction conditions (Figure 3c).

Due to continuous circulation of catholyte in the flow cell setup, the GDL electrode became vulnerable to flooding. Flooded electrodes produced mostly H_2 (Figure S13, Supporting Information), the result of a lack of CO mass transport to CP catalyst. We then sought to run CO-to-acetate conversion using a membrane electrode assembly (MEA) electrolyzer – a catholyte-free system that mitigates flooding.[37] The MEA also has the benefit of lower overall cell resistance than that of a flow cell. Iridium oxide (IrO_2) supported on a titanium mesh, a commercial anion exchange membrane (AEM) and CP catalyst deposited on a GDL were used as the anode, membrane and cathode, respectively (Figure S14a, details in the Supporting Information). The liquid products from both the anode and cathode were analyzed and quantified.[38] The AEM-based MEA (AEM-MEA) enabled stable CORR electrolysis for 200 h at a current density of 160 mA cm^{-2} with a stable acetate FE > 50% (Figure S15a, Supporting Information). Isotopic experiments employing labelled ^{13}CO as the reactant were carried out, and these suggest CO is the reactant (Figure S14b and Figure S15c, Supporting Information). Activity comparisons of acetate and C_2H_4 further suggests different reaction mechanism on CP and control catalysts after C–C coupling (Figure S16, Supporting Information). We further characterized CP catalyst upon completion of 200-h of continuous electrolysis and found no significant change in the chemical, morphological and electronic properties (Figures S17 and S18, Supporting Information). Markedly different product distributions among pure CP catalyst, composite CP catalyst with Cu nanoparticles, and pure Cu nanoparticles in AEM-MEA tests indicate the above performance of CP catalyst is unlikely a result from any leftover Cu impurities (Table S5–S7, Supporting Information). However, over 90% of the produced acetate was collected in the anolyte, due to crossover of acetate anions through the AEM. Acetate in the anolyte could be further oxidized to CO_2 by the anode, which likely explains the slight decrease in the acetate FE with time. Also, the concentration of acetate was low in the anolyte (≈0.04 M), which translates to higher down-stream separation costs,[39,40] therefore motivating strategies for acetate electrosynthesis at high concentrations.
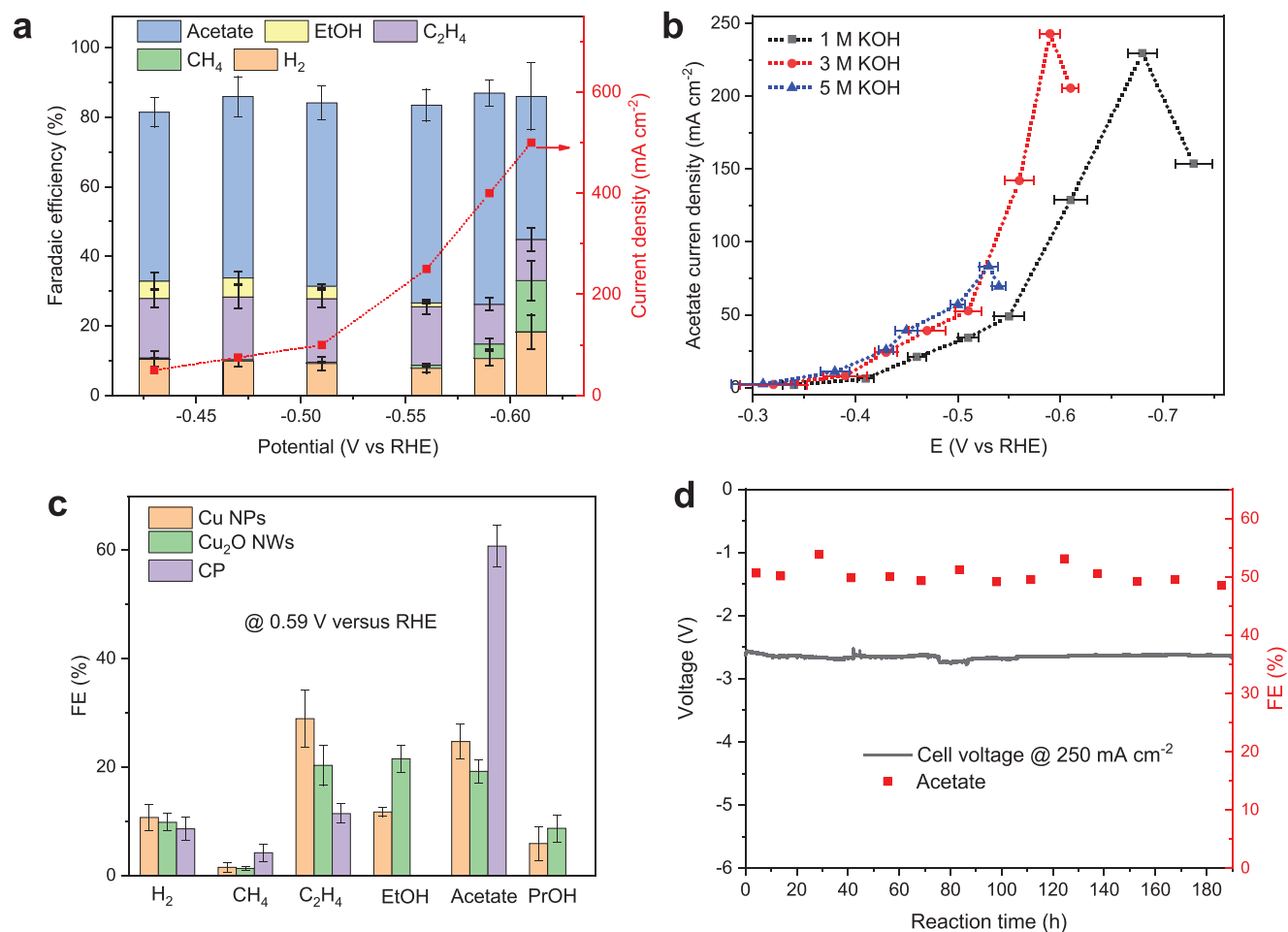
Figure 3. Electrocatalytic CORR performance of CP catalyst in flow cell and membrane electrode assembly configurations. a) Current density and Faradaic efficiency (FE) as a function of applied potential for CORR on CP catalyst in 3 M KOH. b) Acetate current density versus applied potential in various KOH concentrations. c) Product distribution for the cases of CP catalyst, commercial Cu nanoparticles and Cu$_2$O nanowires at −0.59 V versus RHE. d) Cell voltage and FE of acetate (only from the cathodic liquid stream) versus reaction time in MEA with a cation exchange membrane.

Inspired by Kanan and co-workers,[21] we replaced the AEM with a CEM in the MEA system – a strategy to minimize the crossover of acetate produced at the cathode to the anode (Figure S14b, Supporting Information). Potassium cations and water molecules are transported from the anode to the cathode and then couple with acetate anions to form potassium acetate, which can be directly collected as a liquid phase from the cathodic manifold outlet. With this CEM-MEA system, we demonstrated continuous acetate electrosynthesis using the CP catalyst for over 190 h with a stable cell voltage and an average acetate selectivity of 51% at a current density of 250 mA cm^{-2} (Figure 3d). Over the course of 190-h of continuous operation, we collected ≈290 mL of liquid product from the cathode, in which the acetate concentration was 3.3 M. The system also delivered an average acetate full-cell EE of 15%, single-pass utilization (SPU) of 50% for CO-to-acetate conversion, and an acetate partial current density of ≈128 mA cm^{-2} throughout (Table S8, Supporting Information).

We further sought to increase the total C$_2$ productivity (ideally by simultaneously promoting two products – one that can be readily collected in the gas phase (ethylene), the other

separately collected in the liquid phase, i.e., acetate) while maintaining similar, if not increased, productivity, single-pass utilization, and cathodic stream concentration toward acetate. To this end, we fabricated a composite cathode based on CP catalyst versus Cu NPs (details in Supporting Information). In the CEM-MEA system, this composite cathode enabled a combined partial current density of 200 mA cm^{-2} (≈120 mA cm^{-2} towards acetate and ≈80 mA cm^{-2} toward ethylene) with an average single-pass CO-to-(acetate + ethylene) conversion of ≈60% over a course of 250-hour continuous electrolysis (Figure S19 and Table S9, Supporting Information). The system maintained a 22% average full-cell EE towards the sum of {acetate + ethylene}. Upon completion of 250-h continuous electrolysis at 300 mA cm^{-2}, we collected ≈340 mL of liquid product, in which the acetate concentration was 2.9 M.

2.4. Density Functional Theory Calculations

We then employed DFT calculations to explore the origins of selectivity toward CO-to-acetate conversion on the CP catalyst.
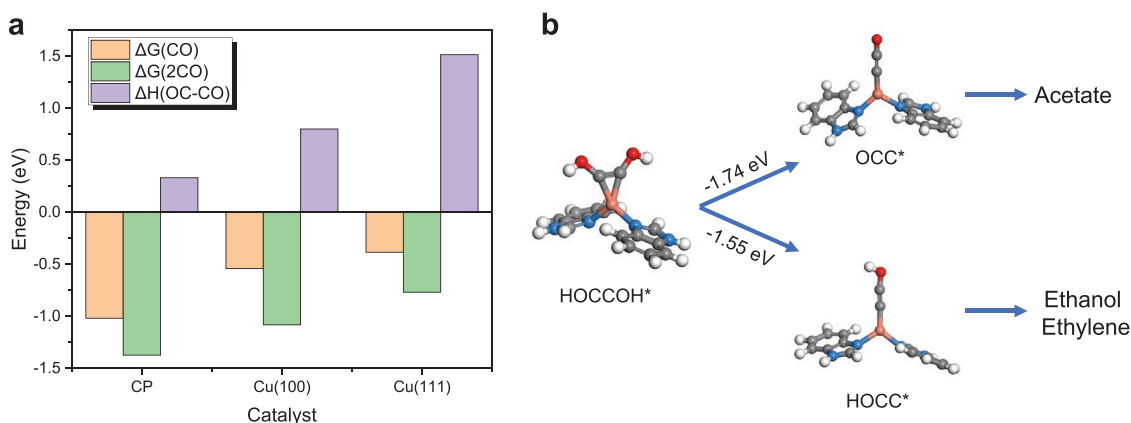
**ADVANCED
SCIENCE NEWS**

www.advancedsciencenews.com

**ADVANCED
MATERIALS**

www.advmat.de

Figure 4. Density functional theory calculations. a) Adsorption energies of one CO and two CO and the enthalpy changes of CO dimerization on the CP, Cu(100), and Cu(111). b) The geometries and energies of branching reactions of acetate and ethanol/ethylene on CP catalyst.

Two possible catalytic sites of the CP structure are the isolated Cu site and the bidentate Cu–N site. We first screened the energetics of adsorption geometries of the possible intermediates, including CO*, CCO*, CCOH*, HOCCOH* (Figures S20–S23, Supporting Information), on these two types of sites, and found three stable configurations of 2CO* (Figure S20a, Supporting Information). From calculation, the most stable configuration is 2CO* on the isolated Cu site, with adsorption configurations involving the adjacent N site less stable.

To query whether C–C coupling could occur on the isolated Cu(I) site, we calculated the adsorption free energy of one and two CO adsorbates on isolated Cu(I) site of CP catalyst, Cu(100), and Cu(111) (**Figure 4**a; Figures S24–S26 and Table S10, Supporting Information). The adsorption free energy of CO on CP catalyst is lower than that of both Cu(100) and Cu(111), suggesting more favorable CO binding on isolated Cu(I) site. The adsorption of two CO molecules is energetically more stable than that of one CO. We then calculated the enthalpy change of CO dimerization – one key C–C coupling step.[41–44] Based on the enthalpy change, we found that CO dimerization on the CP is more favorable compared to those on Cu(100) and Cu(111). The stronger CO binding and better C–C coupling agree with the temperature-programmed desorption of CO (CO-TPD) data (Figure S27, Supporting Information) and CO_2 electroreduction results (Figure S28, Supporting Information). We calculated the hydrogen adsorption energy in this system, and found that HER was unfavorable on CP catalyst (Table S11, Supporting Information). Control experiments with poly-benzimidazole and Ag(I)-CP catalysts suggest that the copper site in the CP catalyst is required for carbonaceous product generation from CORR (Tables S12 and S13, Supporting Information).

Next, we implemented calculations based on a mechanism proposed by Goddard, Jiao, and co-workers.[16] As seen in Figure 4b, the key intermediate branching toward acetate and other products is HOCCOH*. Dehydration of HOCCOH* to OCC* leads to acetate, while the hydrogenation of HOCCOH* to HOCC* gives rise to other C_{2+} products, such as ethanol and ethylene. We calculated the enthalpy changes of the two pathways on CP catalyst, and found that the acetate pathway is more favorable, supporting the high selectivity toward acetate. Notably, recent single-crystal-electrode evidence showed that low-coordinated defects enable the electrosynthesis of C_{2+} products.[45] Others have found evidence that single-metal-site electrocatalysts can enable the coupling (and reversible cleaving) of C−C bonds as well as of H−H, O−O, and N−N bonds.[46] Full mechanistic elucidation of the experimental observations herein will require future studies involving in-situ as well as direct observation of C_2 intermediates.

In summary, we present a Cu(I)-benzimidazole coordination polymer (CP) electrocatalyst for efficient CO-to-acetate conversion. In a flow cell, the CP catalyst enabled a 61% Faradaic efficiency toward acetate at a current density of 400 mA cm^{-2}. When we applied this in a cation exchange membrane-based membrane electrode assembly, we achieved acetate electrosynthesis stable over 190 h, with a concentration of 3.3 molar, a single-pass utilization of 50%, and a full-cell energy efficiency of 15% at a current density of 250 mA cm^{-2}. The findings suggest the need for further study of transition metal-coordination polymers in electrocatalysis.

Supporting Information

Supporting Information is available from the Wiley Online Library or from the author.

Acknowledgements

Conflict of Interest

The authors declare no conflict of interest.

Author Contributions

M.L., A.O., Z.W., F.L., and J.E.H. contributed equally to this work. E.H.S. and D.S. supervised the project. M.L. designed and carried out most of the experiments. A.O. carried out the MEA tests. Z.W. and R.L. designed and carried out the DFT calculations. F.L., J.H., A.O., and S.Z. carried out Raman spectroscopy and part of the electrochemical tests. S.F.H., J.L., D.H.N., and Y.R. carried out the XAS test and analysis. Y.W. and Y.L. synthesized Cu_2O nanowires and carried out SEM imaging. B.C. carried out TEM imaging and elemental mapping. J.W. carried out the XPS measurements. F.W. and H.L. carried out CO-TPD and ICP-AES tests. F.L., S.Z., and D.A. carried out the THz measurements. H.C., Y.R., and L.F. carried out the XRD test. M.L. drafted the manuscript. Y.C.L., Y.X., Y.W.L., and C.T.D. edited the manuscript. All authors discussed the results and assisted during manuscript preparation.

Code Availability

The Vienna ab initio simulation package (VASP) used for the DFT calculations is available at https://www.vasp.at.

Data Availability Statement

The data that support the findings of this study are available from the corresponding author upon reasonable request.

Keywords

acetate, coordination polymers, CO/CO_2 reduction, electrosynthesis, MEA

[1] P. De Luna, C. Hahn, D. Higgins, S. A. Jaffer, T. F. Jaramillo, E. H. Sargent, *Science* **2019**, *364*, eaav3506.

[2] S. Nitopi, E. Bertheussen, S. B. Scott, X. Liu, A. K. Engstfeld, S. Horch, B. Seger, I. E. L. Stephens, K. Chan, C. Hahn, J. K. Nørskov, T. F. Jaramillo, Ib Chorkendorff, *Chem. Rev.* **2019**, *119*, 7610.

[3] C. W. Li, J. Ciston, M. W. Kanan, *Nature* **2014**, *508*, 504.

[4] Y. Y. Birdja, E. Pérez-Gallent, M. C. Figueiredo, A. J. Göttle, F. Calle-Vallejo, M. T. M. Koper, *Nat. Energy* **2019**, *4*, 732.

[5] C. Chen, J. F. Khosrowabadi Kotyk, S. W. Sheehan, *Chem* **2018**, *4*, 2571.

[6] H. Mistry, A. S. Varela, S. Kühl, P. Strasser, B. R. Cuenya, *Nat. Rev. Mater.* **2016**, *1*, 16009.

[7] A. Bagger, W. Ju, A. S. Varela, P. Strasser, J. Rossmeisl, *ACS Catal.* **2019**, *9*, 7894.

[8] J. M. Spurgeon, B. Kumar, *Energy Environ. Sci.* **2018**, *11*, 1536.

[9] M. B. Ross, P. De Luna, Y. Li, C.-T. Dinh, D. Kim, P. Yang, E. H. Sargent, *Nat. Catal.* **2019**, *2*, 648.

[10] K. P. Kuhl, E. R. Cave, D. N. Abram, T. F. Jaramillo, *Energy Environ. Sci.* **2012**, *5*, 7050.

[11] X. Wang, J. F. De Araújo, W. Ju, A. Bagger, H. Schmies, S. Kühl, J. Rossmeisl, P. Strasser, *Nat. Nanotechnol.* **2019**, *14*, 1063.

[12] H. D. May, P. J. Evans, E. V. Labelle, *Curr. Opin. Biotechnol.* **2016**, *42*, 225.

[13] E. V. Labelle, H. D. May, *Front Microbiol* **2017**, *8*, 756.

[14] Reports and Data, "Manufacturing process, by application and by end users, and segment forecasts, 2016–2027" https://www.reportsand-data.com/report-detail/acetic-acid-market (accessed: January 2020).

[15] M. Jouny, G. S. Hutchings, F. Jiao, *Nat. Catal.* **2019**, *2*, 1062.

[16] M. Jouny, J.-J. Lv, T. Cheng, B. H. Ko, J.-J. Zhu, W. A. Goddard, F. Jiao, *Nat. Chem.* **2019**, *11*, 846.

[17] W. Luc, X. Fu, J. Shi, J.-J. Lv, M. Jouny, B. H. Ko, Y. Xu, Q. Tu, X. Hu, J. Wu, Q. Yue, Y. Liu, F. Jiao, Y. Kang, *Nat. Catal.* **2019**, *2*, 423.

[18] D. Karapinar, N. T. Huan, N. Ranjbar Sahraie, J. Li, D. Wakerley, N. Touati, S. Zanna, D. Taverna, L. H. Galvão Tizei, A. Zitolo, F. Jaouen, V. Mougel, M. Fontecave, *Angew. Chem., Int. Ed.* **2019**, *58*, 15098.

[19] Z. Weng, Y. Wu, M. Wang, J. Jiang, K. Yang, S. Huo, X.-F. Wang, Q. Ma, G. W. Brudvig, V. S. Batista, Y. Liang, Z. Feng, H. Wang, *Nat. Commun.* **2018**, *9*, 415.

[20] D.-H. Nam, O. S. Bushuyev, J. Li, P. De Luna, A. Seifitokaldani, C.-T. Dinh, F. P García De Arquer, Y. Wang, Z. Liang, A. H. Proppe, C. S. Tan, P. Todorović, O. Shekhah, C. M. Gabardo, J. W. Jo, J. Choi, M.-J. Choi, S.-W. Baek, J. Kim, D. Sinton, S. O. Kelley, M. Eddaoudi, E. H. Sargent, *J. Am. Chem. Soc.* **2018**, *140*, 11378.

[21] M. L. Lewis, L. Ledung, K. T. Carron, *Langmuir* **1993**, *9*, 186.

[22] S. Zhong, X. Yang, Z. Cao, X. Dong, S. M. Kozlov, L. Falivene, J.-K. Huang, X. Zhou, M. N. Hedhili, Z. Lai, K.-W. Huang, Y. Han, L. Cavallo, L.-J. Li, *Chem. Commun.* **2018**, *54*, 11324.

[23] D. S. Ripatti, T. R. Veltman, M. W. Kanan, *Joule* **2019**, *3*, 240.

[24] L. Martin, H. Martinez, D. Poinot, B. Pecquenard, F. Le Cras, *J. Phys. Chem. C* **2013**, *117*, 4421.

[25] I. J. Pickering, G. N. George, C. T. Dameron, B. Kurz, D R. Winge, I. G. Dance, *J. Am. Chem. Soc.* **1993**, *115*, 9498.

[26] M. Giorgetti, M. Pellei, G. Lobbia, C. Santini, *J. Phys.: Conf. Ser.* **2009**, *190*, 012146.

[27] D. P. Drolet, D. M. Manuta, A. J. Lees, A. D. Katnani, G. J. Coyle, *Inorg. Chim. Acta* **1988**, *146*, 173.

[28] A. Suwaiyan, R. Zwarich, N. Baig, *J Raman Spectrosc* **1990**, *21*, 243.

[29] T. Yoshida, *Bull. Chem. Soc. Jpn* **1980**, *53*, 1449.

[30] G. Xue, J. Ding, P. Wu, G. Ji, *J. Electroanal. Chem. Interf. Electrochem.* **1989**, *270*, 163.

[31] F. Li, A. Thevenon, A. Rosas-Hernández, Z. Wang, Y. Li, C. M. Gabardo, A. Ozden, C. T. Dinh, J. Li, Y. Wang, J. P. Edwards, Y. Xu, C. Mccallum, L. Tao, Z.-Q. Liang, M. Luo, X. Wang, H. Li, C. P. O'brien, C.-S. Tan, D.-H. Nam, R. Quintero-Bermudez, T.-T. Zhuang, Y. C. Li, Z. Han, R. D Britt, D. Sinton, T. Agapie, J. C. Peters, E. H. Sargent, *Nature* **2020**, *577*, 509.

ADVANCED
SCIENCE NEWS
www.advancedsciencenews.com

ADVANCED
MATERIALS
www.advmat.de

[32] Y. Xia, Y. Xiong, B. Lim, S. E. Skrabalak, *Angew. Chem., Int. Ed.* **2008**, *48*, 60.

[33] M. Jouny, W. Luc, F. Jiao, *Nat. Catal.* **2018**, *1*, 748.

[34] J. Li, Z. Wang, C. Mccallum, Y. Xu, F. Li, Y. Wang, C M. Gabardo, C.-T. Dinh, T.-T. Zhuang, L. Wang, J. Y. Howe, Y. Ren, E. H. Sargent, D. Sinton, *Nat. Catal.* **2019**, *2*, 1124.

[35] Y. Pang, J. Li, Z. Wang, C.-S. Tan, P.-L. Hsieh, T.-T. Zhuang, Z.-Q. Liang, C. Zou, X. Wang, P. De Luna, J. P. Edwards, Y. Xu, F. Li, C.-T. Dinh, M. Zhong, Y. Lou, D. Wu, L.-J. Chen, E. H. Sargent, D. Sinton, *Nat. Catal.* **2019**, *2*, 251.

[36] T. Cheng, A. Fortunelli, W. A. Goddard, *Proc Natl Acad Sci USA* **2019**, *116*, 7718.

[37] D. Higgins, C. Hahn, C. Xiang, T. F. Jaramillo, A. Z. Weber, *ACS Energy Lett.* **2018**, *4*, 317.

[38] C. M. Gabardo, C. P. O'brien, J. P. Edwards, C. Mccallum, Y. Xu, C.-T. Dinh, J. Li, E. H. Sargent, D. Sinton, *Joule* **2019**, *3*, 2777.

[39] C. Pirola, F. Galli, F. Manenti, M. Corbetta, C. L. Bianchi, *Ind. Eng. Chem. Res.* **2014**, *53*, 18063.

[40] P. Zhu, C. Xia, C.-Y. Liu, K. Jiang, G. Gao, X. Zhang, Y. Xia, Y. Lei, H. N. Alshareef, T. P. Senftle, H. Wang, *Proc. Natl. Acad. Sci. USA* **2021**, *118*, e2010868118.

[41] E. Pérez-Gallent, M. C. Figueiredo, F. Calle-Vallejo, M T. M. Koper, *Angew. Chem., Int. Ed.* **2017**, *56*, 3621.

[42] J. D. Goodpaster, A. T. Bell, M. Head-Gordon, *J. Phys. Chem. Lett.* **2016**, *7*, 1471.

[43] J. H. Montoya, C. Shi, K. Chan, J. K. Nørskov, *J. Phys. Chem. Lett.* **2015**, *6*, 2032.

[44] X. Liu, P. Schlexer, J. Xiao, Y. Ji, L. Wang, R. B. Sandberg, M. Tang, K. S. Brown, H. Peng, S. Ringe, C. Hahn, T. F. Jaramillo, J. K. Nørskov, K. Chan, *Nat. Commun.* **2019**, *10*, 32.

[45] F. Scholten, K-L. C. Nguyen, J. P. Bruce, M. Heyde, B. Roldan Cuenya, *Angew. Chem., Int. Ed.* **2021**, *60*, 19169.

[46] Y. Wang, H. Su, Y. He, L. Li, S. Zhu, H. Shen, P. Xie, X. Fu, G. Zhou, C. Feng, D. Zhao, F. Xiao, X. Zhu, Y. Zeng, M. Shao, S. Chen, G. Wu, J. Zeng, C. Wang, *Chem. Rev.* **2020**, *120*, 12217.